Supporting Information

Köpper et al. 10.1073/pnas.1304355110

SI Materials and Methods

Cell Culture, Transfection, Chemicals, and Treatments. U2OS cells were cultured in DMEM (Gibco/Life Technologies) supplemented with 10% FCS and antibiotics. For siRNA-mediated knockdown, U2OS cells were reverse-transfected with 5 or 10 nM predesigned Silencer Select siRNAs or control siRNA (all Ambion/Life Technologies) using Lipofectamine 2000 (Invitrogen/Life Technologies). Chemotherapeutic treatment was performed using gemcitabine (Gemzar; Eli Lilly), dissolved in H_2O. Hydroxyurea (HU; Sigma-Aldrich) was also dissolved in H_2O. Controls were treated with the same amount of H_2O. MAP kinase-activated protein kinase 2 (MK2) and Chk1 kinases were inhibited by using 10 μM MK2 Inhibitor III or 2.5 μM SB218078 (both Calbiochem/Merck) dissolved in DMSO as a stock, respectively. Nutlin-3 (Sigma-Aldrich), dissolved in DMSO as a stock, was applied at a concentration of 10 or 20 μM. Controls for inhibitors were treated with DMSO. UV irradiation was administered by using a CL-1000 UV cross-linker (UVP).

High-Content Immunofluorescence Microscopy. Cells were grown in 96-well imaging plates (Becton Dickinson) for 24 h, and then treated as indicated. After fixation in 4% paraformaldehyde in PBS solution, immunofluorescence staining was performed by using the following antibodies in PBS solution containing 10% FCS: mouse anti-γH2AX (JBW301; Millipore/Merck), mouse anti-cyclobutane pyrimidine dimer (TDM-2; Cosmo Bio), mouse anti-BrdU (MoBu-1; Abcam), and Alexa Fluor-488 anti-rabbit and Alexa Fluor-546 anti-mouse (both Invitrogen/Life Technologies). Nuclei were stained with Hoechst 33342 (5 μg/mL; Invitrogen/Life Technologies). Actively replicating cells were identified by labeling with 5 μM 5-ethynyl-2′-deoxyuridine (EdU) by using the Click-iT EdU Alexa Fluor 488 HCS Assay (Life Technologies) or by labeling with 10 μM BrdU (Becton Dickinson). For detection of incorporated BrdU, DNA was denatured with 2 M HCl after permeabilization. All assays were performed in triplicates. Automated microscopy was performed with a Pathway HT Cell Imaging System using the AttoVision image acquisition software (Becton Dickinson), and single-cell-based image analysis. The Hoechst signal was used to identify cell nuclei. For quantification of signal intensities, the average fluorescence resulting from the respective staining was determined per nucleus. For analysis of replicating cells only, cells were gated according to EdU signal intensity, followed by quantification of the γH2AX signal.

High-Content Automated Cell Screening. Automated transfection was performed by using a Biomek 3000 laboratory automation workstation (Beckman Coulter). Cells were reverse-transfected with the Silencer Human Kinase siRNA Library V3 (Ambion) targeting the human kinome in 96-well imaging plates as detailed earlier. The final siRNA concentration was 30 nM. The library contains three different siRNAs per target gene on separate plates. At 48 h after transfection, cells were irradiated with 20 J/m^2 UV-C and fixed after 2.5 h. Staining was with Hoechst and for γH2AX, and automated microscopy and image analysis were performed as described earlier.

Statistical Analysis. For statistical analysis of the screen, sample-based normalization was used. In short, for each plate, the median and median absolute deviation were calculated from the average γH2AX intensities of all wells. The robust *z*-score was calculated to determine the effect each siRNA had on the accumulation of γH2AX. The sum of the *z*-scores of the three siRNAs used for each gene of interest was calculated, and the genes were ranked according to this cumulative *z*-score.

If not stated otherwise, data from other experiments are shown as mean ± SD. Unpaired Student *t* test was used for the calculation of *P* values. *n* values in figure legends indicate the number of independent replicates.

Immunoblotting and Antibodies. Cell lysates were separated by SDS polyacrylamide gel electrophoresis and transferred to nitrocellulose membranes. For detection of specific proteins, the membranes were incubated with antibodies diluted in 5% BSA in Tris-buffered saline solution containing 0.1% Tween-20. The following primary antibodies were used: rabbit anti-MK2, rabbit anti-JNK pT183pY185, rabbit anti-MK2, mouse anti-Chk1 (all Cell Signaling Technology), mouse anti-γH2AX (JBW301; Millipore/Merck), mouse anti-PARP1 (C-2-10; Calbiochem/Merck), mouse anti–β-actin (AC-15; Abcam), rabbit anti-Hsp27 pS82 (E118; Abcam), and mouse anti-hsc70 (B_6; Santa Cruz Biotechnology). Primary antibodies were detected with peroxidase-coupled secondary antibodies (Jackson ImmunoResearch Europe).

UV Irradiation of Mice and Immunohistochemistry. MK2 KO and MK2/MK3 double KO (DKO) mice have been described before (1, 2). The animal studies have been approved by the Animal Protection Commission of the Faculty of Medicine, University of Göttingen.

UV irradiation. The depilated backs of WT ($n = 5$) and MK2/MK3-deficient ($n = 6$) mice were exposed to UV-B irradiation (250 mJ/cm^2). Areas of 2 cm^2 each on the backs of the MK2/MK3 DKO mice were protected from irradiation by using a lightproof aluminum cover. In addition, five WT mice were not irradiated. Mice were euthanized 24 h after irradiation, and both irradiated and nonirradiated dorsal skin samples were processed for immunohistochemistry. Samples were fixed in 4% (vol/vol) paraformaldehyde and paraffin-embedded, and 4 μm sections were cut.

TUNEL assay. Apoptotic cells were detected by using a modified TUNEL assay (DermaTACS; R&D Systems). One tissue section in each experiment was treated with TACS nuclease (positive control with DNA fragmentation in all cells), and in one section terminal desoxynucleotidyl transferase was omitted (negative control). TUNEL-positive cells were quantitated microscopically using an Axioscope 2 Plus and AxioVision 3.0 image analysis software (Zeiss). The entire tissue sections were used to quantify TUNEL-positive cells. MK2 KO mice were treated and analyzed identically.

Proliferation Assay. For cell proliferation analysis using kinase inhibitors, cells were seeded in triplicate in 96-well plates and, after 24 h, treated with the respective inhibitors and drugs for 24 h. For cell proliferation analysis with siRNA-mediated knockdown, cells were reverse-transfected with siRNA and reseeded at equal density in triplicate in 96-well plates 48 h later. Cell confluence was measured on consecutive days by bright-field microscopy by using a Celigo Adherent Cell Cytometer (Brooks Automation).

Clonogenic Assay. Cells were reverse-transfected with siRNA as described earlier. At 48 h later, the cells were irradiated with UV-C light and reseeded at equal density. After 15 d, for colony staining, the cells were washed with PBS solution, fixed in 70% methanol at −20 °C, and stained with crystal violet solution (10% formaldehyde, 1 mg/mL crystal violet) for 30 min. Colony density was analyzed by quantification of the stained area by using Fiji software (http://fiji.sc/wiki/index.php/Fiji).

Flow Cytometry. For analysis by flow cytometry, cells were harvested, fixed in ethanol, and stained with propidium iodide. Cell cycle profiles were generated using a Guava EasyCyte Plus system (Millipore/Merck) and analyzed by using ModFit LT software (Verity Software House).

Confocal Microscopy. Overexpression of MK2 was induced by transfection of a pcDNA3 Myc-MK2 expression vector (3). After treatment, cells were fixed and stained as described for high-content immunofluorescent microscopy. Myc-tagged MK2 was detected with mouse anti–Myc-tag antibody (Millipore/Merck). Images were acquired by using a confocal microscope (plan apochromatic objective, 63×; 1.4 NA; LSM 510 Meta software, version 4.0; Zeiss) at RT.

DNA Fiber Assay. Analysis of replication fork speed and origin firing was essentially done as described previously (4). Exponentially growing cells were pretreated with chemicals for 1 h as indicated. Afterward, the cells were pulse-labeled with 25 μM 5-chloro-2′-deoxyuridine (CldU) for 20 min, followed by 250 μM 5-iodo-2′-deoxyuridine (IdU; both from Sigma-Aldrich) for 20 min, 1 or 2 h, accompanied by treatment with gemcitabine or inhibitors as indicated. Cells were harvested and DNA fibers were spread on glass slides as described before (5). After acid treatment, CldU- and IdU-labeled tracts were detected by 1 h incubation at 37 °C with rat anti-BrdU antibody (dilution 1:1,000, detects BrdU and CldU; AbD Serotec) and mouse anti-BrdU antibody (1:1,000,detects BrdU and IdU; Becton Dickinson). Slides were fixed in 4% paraformaldehyde and incubated for 2 h at room temperature with Alexa Fluor 555-conjugated goat anti-rat antibody or Alexa Fluor 488-conjugated goat anti-mouse antibody (dilution 1:500; both from Molecular Probes/Life Technologies). Samples were mounted in Vectashield (Vector Laboratories). Fiber images were acquired by confocal microscopy as described earlier. The lengths of CldU- (red) and IdU- (green) labeled fibers were measured by using the Fiji software in micrometers, with those values converted to kb using the conversion factor 1 μm = 2.59 kb (6). Replication structures were quantified by using the Cell Counter Plug-in for Fiji (Kurt De Vos, University of Sheffield, Sheffield, United Kingdom).

ssDNA Assay. Detection of ssDNA labeled with BrdU was essentially done as described previously (7): Cells were incubated with 10 μM BrdU for 24 h and treated as indicated. Before fixation, cells were preextracted for 5 min with 0.5% Triton X-100, 20 mM Hepes, pH 7.5, 300 mM sucrose, 50 mM NaCl, and 3 mM $MgCl_2$. Samples were stained for immunofluorescence as described earlier, and BrdU was detected with mouse anti-BrdU antibody (RPN20AB; Amersham/GE Healthcare). High-content immunofluorescence microscopy was applied to quantify the BrdU signal as described earlier.

RNA Extraction and Quantitative RT-PCR. RNA was isolated from cells by using TRIzol (Invitrogen/Life Technologies). The isolated mRNA was reverse-transcribed by using random hexameric and oligo-dT primers, and SYBR Green (Invitrogen/Life Technologies) was used for quantitative RT-PCR (qRT-PCR) analysis. The qRT-PCR primer sets were as follows: GAPDH, 5′-GAAGGTCGGAGTCAACGGATTTG-3′ and 5′-CAGAGATGATGACCCTTTTGGCTC-3′; PolH, 5′-CCAGTAGGCACCGAACCCAGC-3′ and 5′-CAATTATTCCACCACCCTTCCATG-3′; and Rev3L, 5′-CGCATATTCCCTACCTCCTACAGC-3′ and 5′-TGGTATTTCATCTTGTTCCCACCG-3′. Data were normalized to GAPDH. Relative gene expression was calculated by using the ΔΔCt method.

In Vitro Kinase Assay. Recombinant Pol η protein (1–414 aa; Abnova) was used in a radioactive in vitro kinase assay with [γ-^{33}P]ATP as described previously (8). The reaction mix was subsequently separated on SDS/PAGE gradient gels and transferred to nitrocellulose membranes. Radioactivity incorporated was quantified by phosphoimaging using a Fuji FLA9000. The band intensities were quantified by the ImageJ program (National Institutes of Health).

1. Ronkina N, et al. (2007) The mitogen-activated protein kinase (MAPK)-activated protein kinases MK2 and MK3 cooperate in stimulation of tumor necrosis factor biosynthesis and stabilization of p38 MAPK. *Mol Cell Biol* 27(1):170–181.
2. Kotlyarov A, et al. (1999) MAPKAP kinase 2 is essential for LPS-induced TNF-alpha biosynthesis. *Nat Cell Biol* 1(2):94–97.
3. Engel K, Plath K, Gaestel M (1993) The MAP kinase-activated protein kinase 2 contains a proline-rich SH3-binding domain. *FEBS Lett* 336(1):143–147.
4. Petermann E, Woodcock M, Helleday T (2010) Chk1 promotes replication fork progression by controlling replication initiation. *Proc Natl Acad Sci USA* 107(37): 16090–16095.
5. Jackson DA, Pombo A (1998) Replicon clusters are stable units of chromosome structure: Evidence that nuclear organization contributes to the efficient activation and propagation of S phase in human cells. *J Cell Biol* 140(6):1285–1295.
6. Henry-Mowatt J, et al. (2003) XRCC3 and Rad51 modulate replication fork progression on damaged vertebrate chromosomes. *Mol Cell* 11(4):1109–1117.
7. Syljuåsen RG, et al. (2005) Inhibition of human Chk1 causes increased initiation of DNA replication, phosphorylation of ATR targets, and DNA breakage. *Mol Cell Biol* 25(9): 3553–3562.
8. Menon MB, et al. (2010) p38 MAP kinase and MAPKAP kinases MK2/3 cooperatively phosphorylate epithelial keratins. *J Biol Chem* 285(43):33242–33251.

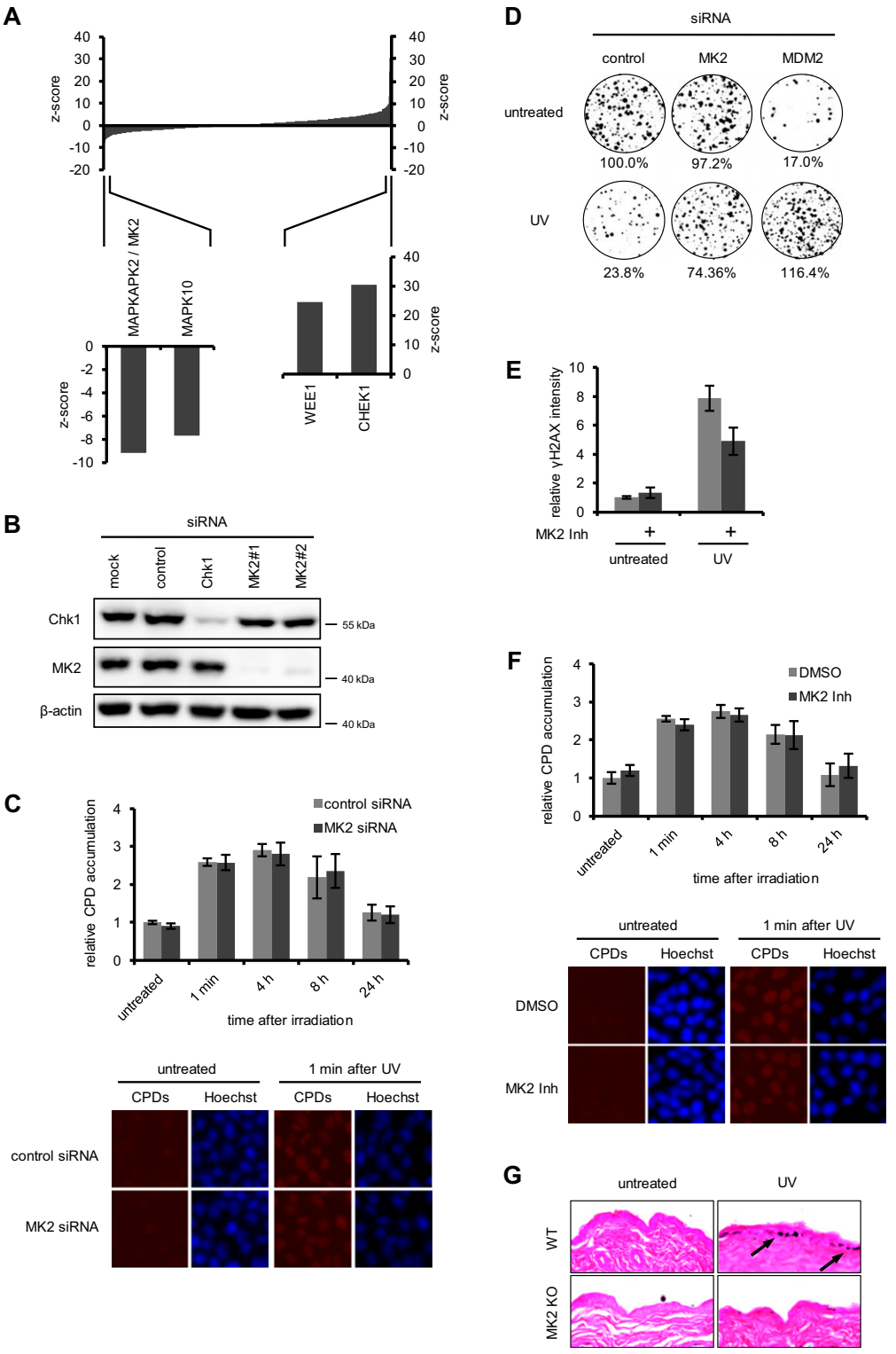

Fig. S1. (*A*) RNAi kinase screen identifies kinases influencing H2AX phosphorylation following UV irradiation. At 48 h after transfection with siRNAs, cells were irradiated with 20 J/m^2 UV-C, fixed 2.5 h later, and stained with Hoechst and anti-γH2AX antibody. Target genes were ranked according to the cumulative robust *z*-score resulting from three separate siRNAs each, reflecting their impact on UV-induced H2AX phosphorylation. The two target genes with the highest and lowest cumulative *z*-scores are shown in magnification. Complete screen results are provided in Dataset S1. (*B*) Depletion efficiencies of Chk1 and MK2 by siRNA-mediated knockdown. Cells were harvested 48 h after knockdown, and protein lysates were analyzed by immunoblotting. (*C*) UV-induced cyclobutane pyrimidine dimer (CPD) accumulation is not affected by MK2 depletion. Cells were depleted of MK2. After 48 h, cells were irradiated with 30 J/m^2 UV-C, fixed at the indicated time points after irradiation, and stained for immunofluorescence analysis, and CPD fluorescence intensity was quantified. Results were normalized to the untreated control transfection and corrected for background fluorescence. Representative images of CPD accumulation without irradiation and 1 min after irradiation are shown. (*D*) MK2 depletion improves cell survival after UV irradiation. Cells were depleted of Mdm2 or MK2. At 48 h later, cells were irradiated with 20 J/m^2 UV-C and reseeded, and cell survival was analyzed by clonogenic assays. Percentages reflect confluence of cells relative to the untreated

Legend continued on following page

control transfection. Note that UV-treated cells were grown for 5 d more before fixation compared with nonirradiated cells, explaining the seeming increase in colonies when Mdm2-siRNA–treated cells were irradiated. (*E*) MK2 inhibition reduces H2AX phosphorylation after UV-induced DNA damage. Cells were preincubated with MK2 inhibitor (MK2 Inh) for 4 h, then irradiated with 600 J/m^2 UV-B. At 2 h later, cells were fixed and stained for immunofluorescence analysis, and γH2AX fluorescence intensity was quantified. Results were normalized to the DMSO-treated control and corrected for background fluorescence. (*F*) UV-induced CPD accumulation is not affected by MK2 inhibition. Cells were treated with MK2 inhibitor for 2 h, then irradiated with 30 J/m^2 UV-C, fixed at the indicated time points after irradiation, stained, and analyzed as in *C*. Results were normalized to the DMSO-treated control transfection and corrected for background fluorescence. Representative images of CPD accumulation without irradiation and 1 min after irradiation are shown. (*G*) MK2 KO mice display reduced apoptosis in skin after UV exposure. Backs of MK2 KO mice and WT animals were exposed to 250 mJ/cm^2 UV-B irradiation or left untreated. Mice were euthanized 24 h after irradiation, and skin samples were processed for immunohistochemistry and stained with eosin (red) and for TUNEL (blue). Representative images are shown.

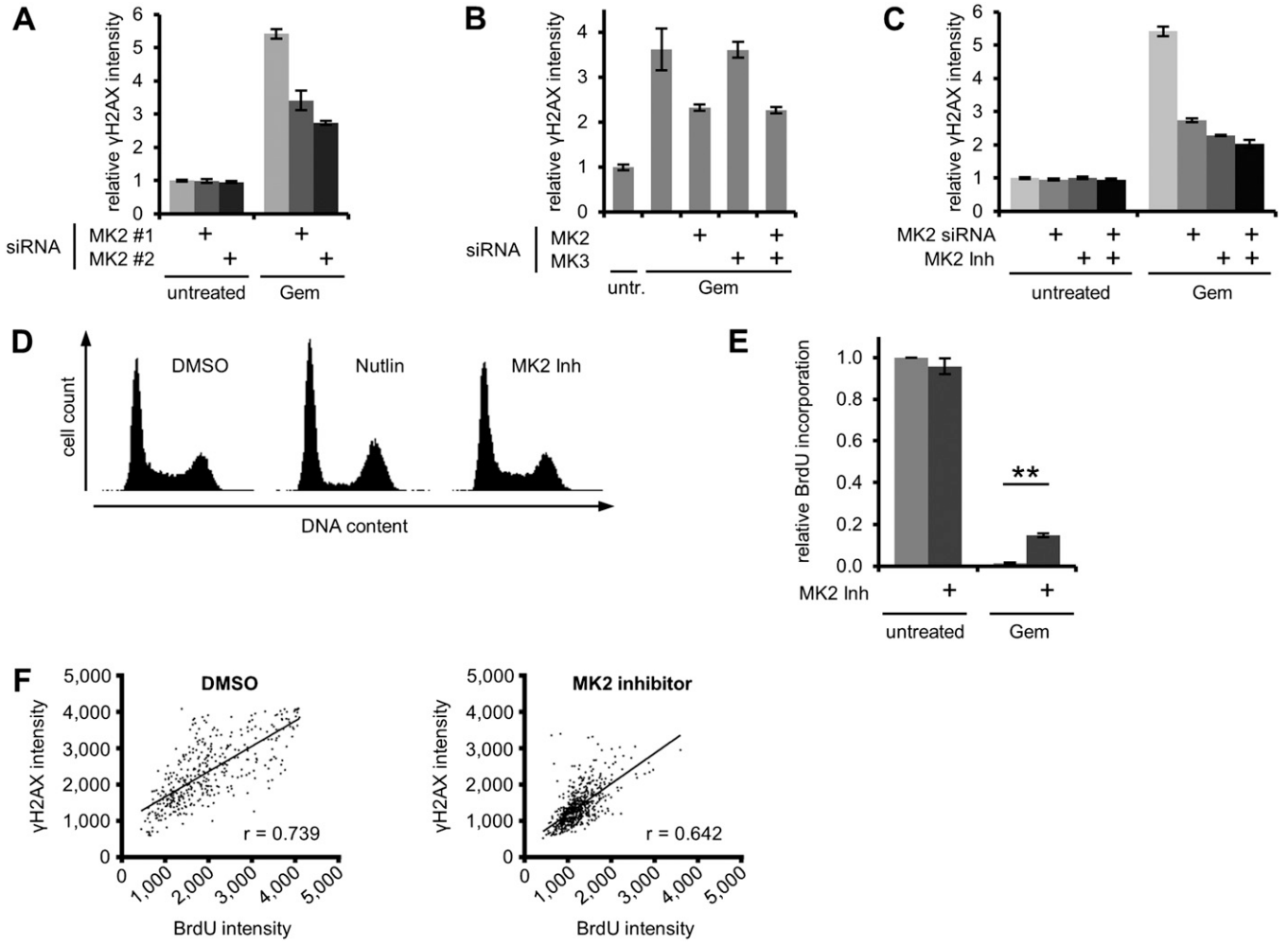

Fig. S2. (*A*) MK2 knockdown reduces gemcitabine-induced γH2AX accumulation. MK2 was depleted with two different siRNAs. Cells were treated with 100 nM gemcitabine for 24 h and stained for immunofluorescence analysis, and γH2AX fluorescence intensity was quantified. (*B*) Gemcitabine-induced γH2AX accumulation depends on MK2 but not MK3. MK2 and MK3 [both present in U2OS (1)] were depleted by siRNA. Cells were treated with 200 nM gemcitabine for 24 h and stained for immunofluorescence analysis, and γH2AX fluorescence intensity was quantified. (*C*) MK2 inhibition and knockdown both efficiently reduce gemcitabine-induced H2AX phosphorylation. Cells were depleted of MK2 and treated with 100 nM gemcitabine for 24 h in the presence of MK2 inhibitor. Cells were stained for immunofluorescence analysis and γH2AX fluorescence intensity was quantified. (*D*) MK2 inhibition does not detectably influence cell cycle distribution. Cells treated with MK2 inhibitor or the Mdm2-antagonist Nutlin-3 (control) for 24 h were subjected to propidium iodide staining and flow cytometry. (*E*) MK2 inhibition improves slow DNA replication upon gemcitabine treatment. Cells treated with 100 nM gemcitabine and/or MK2 inhibitor for 4 h and labeled with BrdU during the last 2 h were fixed and stained for immunofluorescence analysis, and BrdU fluorescence intensity was quantified. Note that, here, unlike in the experiments shown in Fig. 2*G*, Fig. S2*F*, and Fig. S8*B*, the DNA was denatured by 2M HCl treatment before staining, allowing the detection of all BrdU-labeled DNA. Results were normalized to the untreated control and corrected for background fluorescence ($n = 3$; $^{**}P = 0.0014$). (*F*) Gemcitabine-induced H2AX phosphorylation correlates with ssDNA accumulation. BrdU-labeled cells were treated with 300 nM gemcitabine and MK2 inhibitor for 24 h. Cells were fixed and processed for ssDNA quantification by immunofluorescent detection of accessible BrdU and for simultaneous γH2AX quantification (no DNA-denaturation treatment was carried out). γH2AX intensities of regions of interest were plotted against the respective BrdU signal. Image is representative of three independent replicates. The correlation coefficient *r* is given.

1. de Olano N, et al. (2012) The p38 MAPK-MK2 axis regulates E2F1 and FOXM1 expression after epirubicin treatment. *Mol Cancer Res* 10(9):1189–1202.

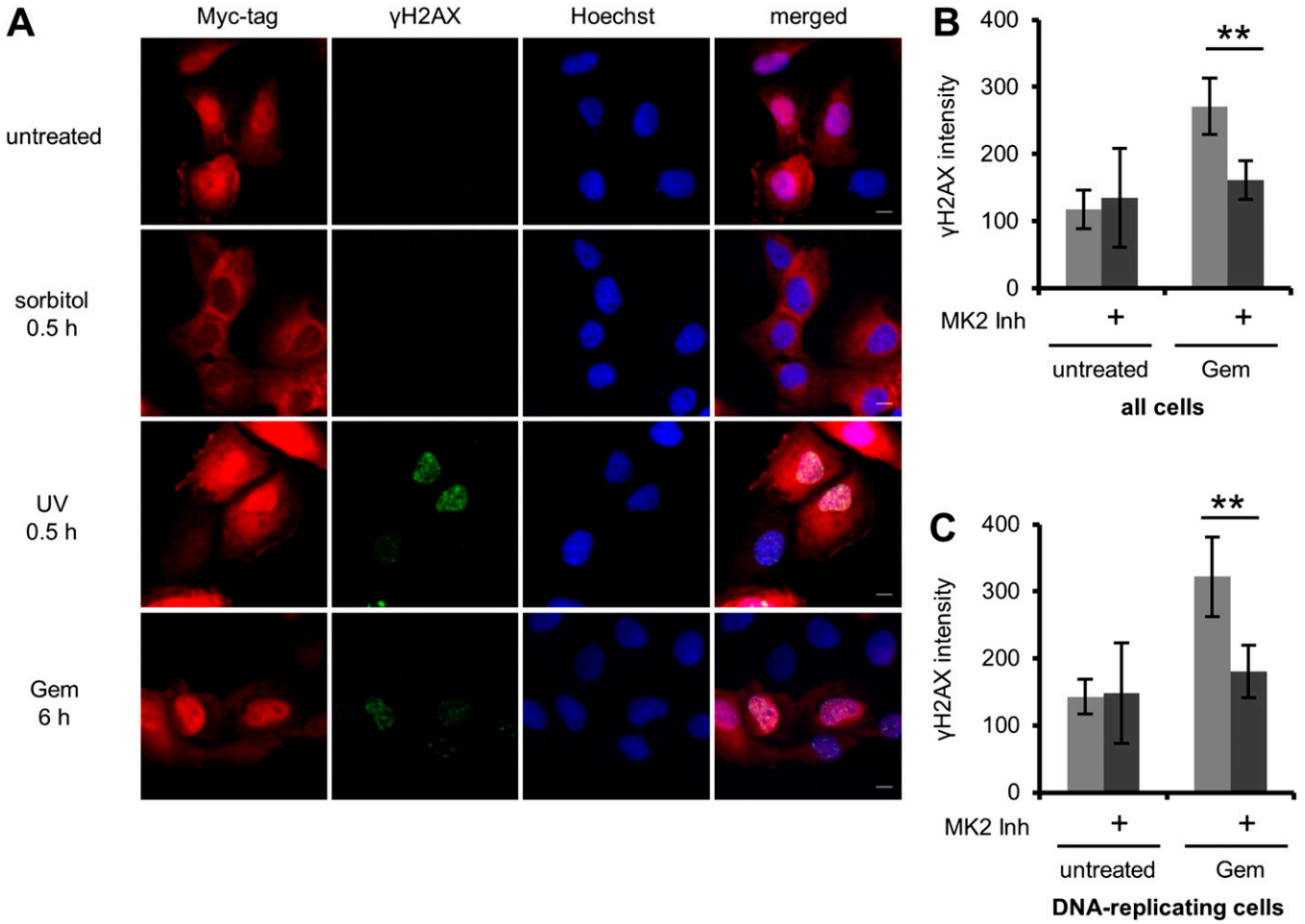

Fig. S3. (*A*) Following genotoxic stress, MK2 is not completely exported from the nucleus. Cells expressing Myc-tagged MK2 were treated with 0.4 M sorbitol, 40 J/m^2 UV-C light, or 100 nM gemcitabine as indicated, or left untreated. Localization of Myc-MK2 and accumulation of γH2AX were analyzed by immunofluorescent confocal microscopy. (Scale bar: 10 μm.) (*B* and *C*) MK2 acts in cells during DNA replication. Cells were treated with MK2 inhibitor for 8 h. Then, replicating cells were labeled with EdU for 2 h. Cells were subsequently treated with 300 nM gemcitabine for 22 h, and γH2AX fluorescence intensity was quantified. (*B*) The average γH2AX fluorescence was determined per nucleus and averaged over all nuclei ($n = 4$; $^{**}P = 0.0057$ and $^{**}P = 0.0051$, respectively). (*C*) Nuclei were gated for EdU fluorescence to identify replicating cells. The average γH2AX fluorescence was determined for these nuclei only ($n = 4$; $^{**}P = 0.0074$).

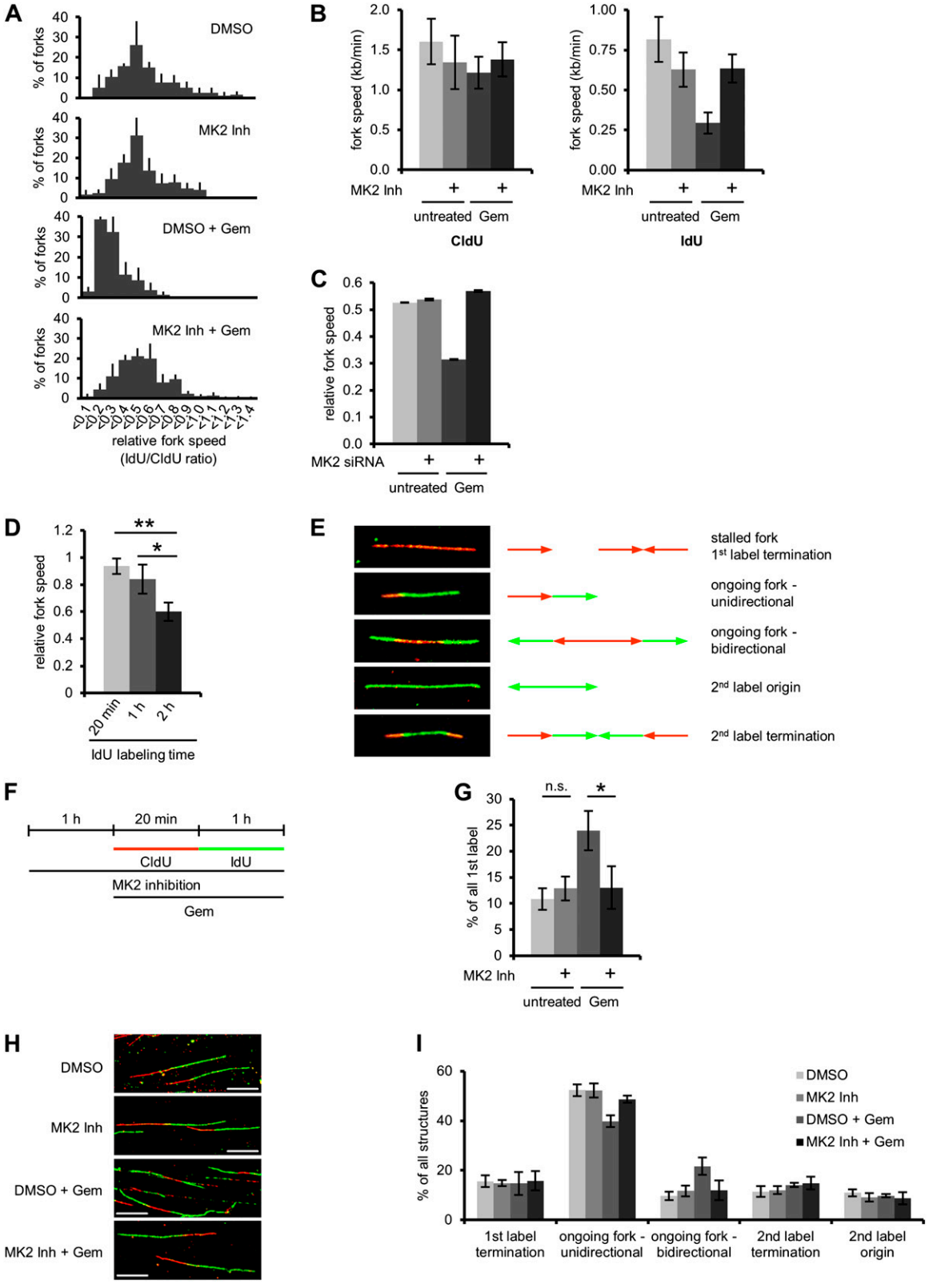

Fig. S4. (*A*) Distribution of replication fork speeds in cells treated as in Fig. 2*D*. (*B*) Average absolute replication fork speed during the CldU and IdU label, respectively, of cells treated as in Fig. 2*D*. Note that only red-green–labeled, unidirectional forks were measured. Therefore, the general stop rate of a replication fork affects only the IdU label in this assay, resulting in a lower overall absolute IdU, but not CldU, fork speed, which translates into a relative fork speed <1 for untreated cells as shown in Fig. 2*E*. The relative fork speed approximates 1 when IdU labeling is reduced to 20 min, as shown in Fig. S4*D*. (*C*) Gemcitabine-induced slow fork speed is rescued by MK2 depletion. Cells were depleted of MK2 and labeled 48 h later with CldU for 20 min and IdU combined with 400 nM gemcitabine for 2 h. Average relative replication fork speed (ratio of length of IdU-labeled vs. length of CldU-labeled tracks) is shown. Error bars

Legend continued on following page

show SE. (*D*) The measured relative fork speed decreases with IdU labeling time. Average relative replication fork speed (ratio of length of IdU-labeled vs. length of CldU-labeled tracks divided by the ratio of IdU vs. CldU labeling time) in cells labeled 20 min with CldU followed by different times of IdU label ($n = 3$; $^{**}P = 0.0028$ and $^{*}P = 0.0309$). Such a nonlinear relationship between track length and labeling period has been observed before (1). The raw data are provided in Dataset S2. (*E*) Images obtained by DNA fiber analysis and schematic representation of structures observed. (Figure modified from ref. 2.) For analysis of replication fork speed, only ongoing (red-green–labeled) forks were measured. For quantification of origin firing, first label origins were counted as percentage of all red-labeled fibers. (*F*) Labeling protocol for DNA fiber analysis of origin firing. U2OS cells were pretreated with MK2 inhibitor for 1 h, then pulse-labeled with CldU and IdU in the presence of 400 nM gemcitabine for 20 min and 1 h, respectively. CldU and IdU were detected as detailed in Fig. 2*D*. (*G*) MK2 inhibition rescues increased origin firing caused by gemcitabine. Quantification of origin firing in cells in dependence of gemcitabine and MK2 inhibition. First label origins (green-red-green fibers) are shown as percentage of all red-labeled fibers ($n = 3$; $^{*}P = 0.0271$). (*H*) Representative images of fibers from cells treated as in *F*. (Scale bar: 10 μm.) (*I*) Quantification of all structures obtained by DNA fiber analysis as detailed in *F*. Note that the frequency of second label origins is not changed in response to gemcitabine treatment. Only-green–labeled structures might also arise from resumed fork elongation during the IdU label, which may obscure increased origin firing, as both result in green-only fibers. Therefore, only unambiguous green-red-green structures were used to determine origin firing frequency.

1. Merrick CJ, Jackson D, Diffley JF (2004) Visualization of altered replication dynamics after DNA damage in human cells. *J Biol Chem* 279(19):20067–20075.
2. Petermann E, Woodcock M, Helleday T (2010) Chk1 promotes replication fork progression by controlling replication initiation. *Proc Natl Acad Sci USA* 107(37):16090–16095.

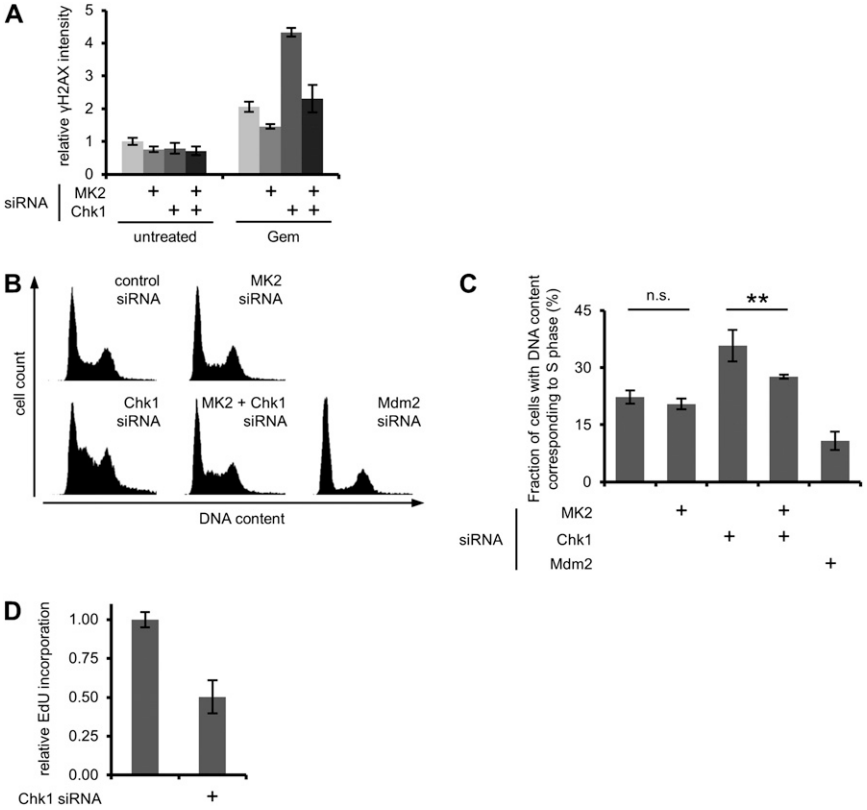

Fig. S5. (*A*) Enhanced γH2AX accumulation by Chk1 depletion upon gemcitabine treatment depends on MK2. Cells were depleted of MK2 and Chk1, treated with 100 nM gemcitabine for 24 h and stained for immunofluorescence analysis. γH2AX fluorescence intensity was quantified. (*B* and *C*) S phase arrest of Chk1-depleted cells is rescued by codepletion of MK2. (*B*) Cells were depleted of MK2, Chk1, and Mdm2 (positive control) and fixed 48 h later. Cell cycle analysis was performed by flow cytometry, quantifying propidium iodide staining. Profiles are representative of four independent replicates. (*C*) The fraction of cells in different phases of the cell cycle was analyzed from the cell cycle profiles shown in *B* ($n = 4$; $^{**}P = 0.0076$). (*D*) Chk1 knockdown induces S phase arrest. Cells were depleted of Chk1. At 42 h later, cells were labeled with EdU for 2 h and stained for immunofluorescence analysis. EdU fluorescence intensity was quantified as a measure for DNA replication.

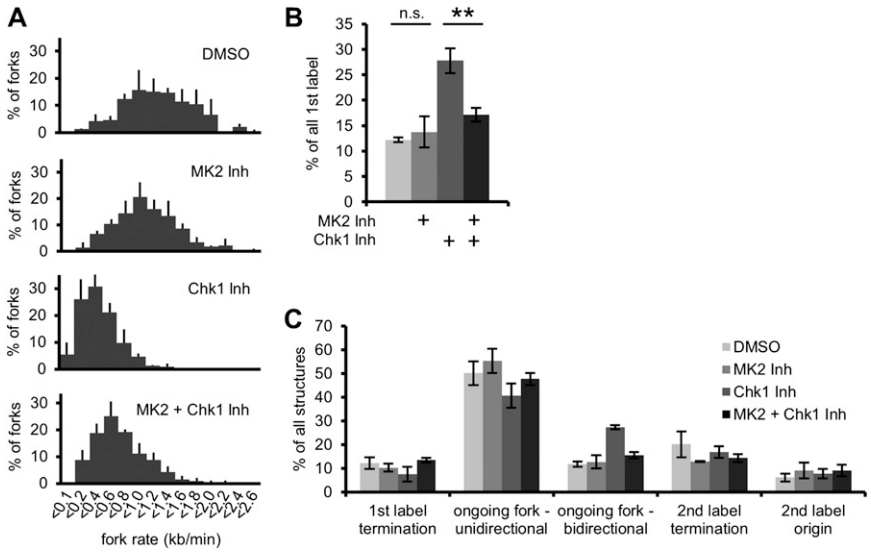

Fig. S6. (*A*) Distribution of replication fork speeds in cells treated as detailed in Fig. 3*D*. (*B* and *C*) MK2 inhibition rescues increased origin firing caused by Chk1 inhibition. Quantification of origin firing in cells upon Chk1 and/or MK2 inhibition. First label origins (green-red-green fibers) are shown as percentage of all red-labeled fibers ($n = 3$; $^{**}P = 0.0027$). (*C*) Quantification of all structures obtained by DNA fiber analysis as detailed in Fig. 3*D*. The legend to Fig. S4*I* specifies the significance of second label origins.

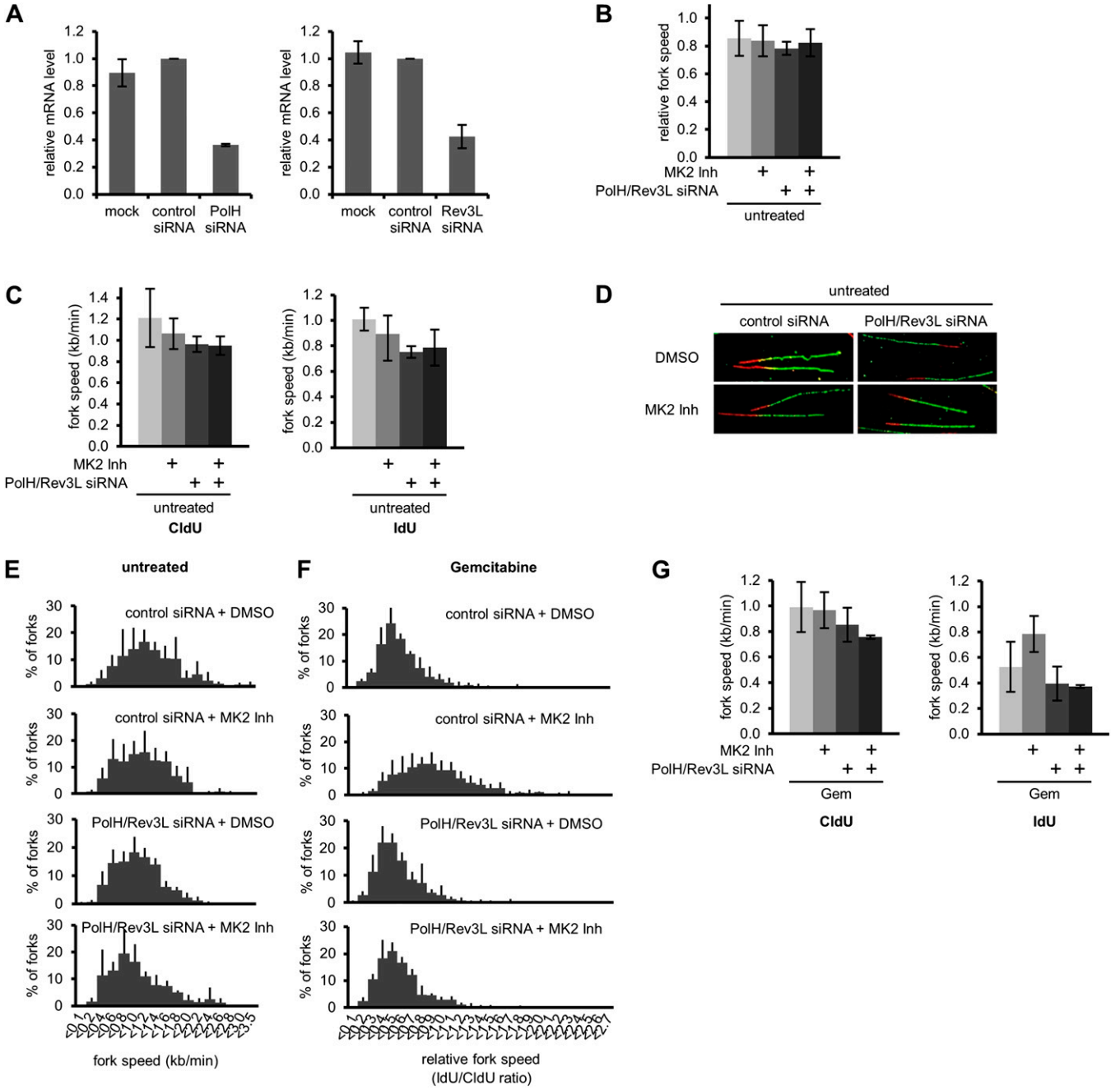

Fig. S7. (*A*) Depletion efficiencies of PolH and Rev3L. Cells were harvested 72 h after knockdown, mRNA was isolated, and mRNA levels were analyzed by quantitative RT-PCR. mRNA levels of PolH and Rev3L were normalized to GAPDH expression ($n = 3$). (*B–E*) Depletion of PolH and Rev3L with or without MK2 inhibition does not detectably change the average replication fork speed in the absence of gemcitabine. Cells were treated as in Fig. 4*A*. (*B*) Average relative replication fork speed in untreated cells in dependence of MK2 inhibition and depletion of PolH and Rev3L. Note that the relative fork speed of control-treated cells is higher than that of the control-treated cells in Fig. 2*E*. This discrepancy might be a result of stress inflicted by siRNA transfection, which might affect fork speed, the average fall-off rate, and the relative influence of gemcitabine. (*C*) Average absolute replication fork speed in untreated cells, in dependence of MK2 inhibition and depletion of PolH and Rev3L. (*D*) Representative images of untreated fibers. (*E*) Distribution of replication fork speeds in untreated cells in dependence of MK2 inhibition and depletion of TLS polymerases polymerase (Pol) η and Rev3L. (*F*) Distribution of replication fork speeds in cells treated with gemcitabine as in Fig. 4*A* in dependence of MK2 inhibition and depletion of TLS polymerases Pol η and Rev3L. (*G*) Average absolute CldU and IdU fork speeds in cells treated with gemcitabine as in Fig. 4*A*. Note that gemcitabine was not present during the CldU label.

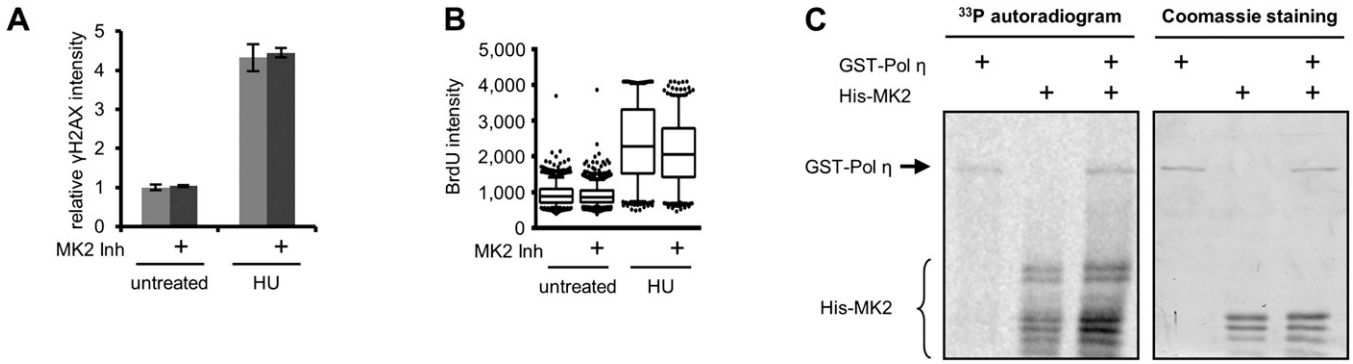

D

Identities = 27/89 (30%), Positives = 41/89 (45%), Gaps = 9/89 (10%)

```
PolH:   206 RETGFQCSAGISHNKVLAKLACGLNKPNRQTLV----SHGSVPQLFSQMPIRKIRSLGGKLGASVIEILGIEYMGELTQ-FTESQLQSH 289
            RE    C   ++H  V+ +    LN P++  +V    S GS+  L  +   ++I  L  KL  +V    G+EY+  LTQ      L SH
TNNI3K: 46 REVSILCQ--LNHPCVIQFVGACLNDPSQFAIVTQYISGGSLFSLLHEQ--KRILDLQSKLIIAVDVAKGMEYLHNLTQPIIHRDLNSH 130
```

Fig. S8. (*A*) H2AX phosphorylation following HU treatment is independent of MK2. Cells were treated with 2 mM HU in the presence of MK2 inhibitor for 20 h, then stained for immunofluorescence analysis, and γH2AX fluorescence intensity was quantified. (*B*) MK2 inhibition does not rescue HU-induced ssDNA formation. BrdU-labeled cells were treated with 2 mM HU and MK2 inhibitor for 24 h. Cells were fixed and processed for ssDNA quantification by immunofluorescent detection of accessible BrdU. (*C*) MK2 enhances Pol η phosphorylation in vitro. Purified GST-tagged Pol η fragment (amino acids 1–414) was incubated with purified His-tagged MK2 in the presence of [γ-^{33}P]ATP. GST-Pol η incubated in the absence of MK2 also yielded a signal in the autoradiogram, suggesting autophosphorylation. Still, in the presence of MK2, the signal intensity increased 1.8-fold. Pol η has been reported to be phosphorylated in response to UV irradiation (1). The phosphorylation site S380 (2) of the Pol η protein is located in a MK2 consensus motif D-K-R-L-S-S*-L. MK2 autophosphorylation was also detected, as reported previously (3). (*D*) As a possible basis for autophosphorylation, BLASTP analysis of Pol η amino acids 1 to 414 using the kinase domain database 4_kinome_domains (www.kinase.com) revealed homology of Pol η amino acids 206 to 289 to the kinase domain of TNNI3K.

1. Chen YW, et al. (2008) Human DNA polymerase eta activity and translocation is regulated by phosphorylation. *Proc Natl Acad Sci USA* 105(43):16578–16583.
2. Bennetzen MV, et al. (2010) Site-specific phosphorylation dynamics of the nuclear proteome during the DNA damage response. *Mol Cell Proteomics* 9(6):1314–1323.
3. Menon MB, et al. (2010) p38 MAP kinase and MAPKAP kinases MK2/3 cooperatively phosphorylate epithelial keratins. *J Biol Chem* 285(43):33242–33251.

Dataset S1. siRNA screen results

Dataset S1

Columns A-L: "#A", "#B", "#C" refers to the three independent siRNAs used per target gene. "Well ID" identifies the siRNA's location on the plate. The three siRNAs of one target gene are always located in the same position on three different plates. "Average intensity" shows intensity of γH2AX staining. "*z*-score" is the robust *z*-score calculated for each individual siRNA. Columns M and N: "plate" identifies the library plate number. "z-score" is the cumulative robust *z*-score, i.e., the sum of the three *z*-scores in columns C, G, K for each target gene. All target genes are sorted according to their cumulative z-score.

Dataset S2. Fiber assay raw data

Dataset S2

(*A*) Fork speed: Length of individual CldU- and IdU-labeled tracks in pixel is given. Micrometer conversion factor (from pixel): 0.13; kb conversion factor (from micrometer): 2.59. (*B*) Origin firing. Total number of observed structures is provided.